Pattern Recognition Letters 29 (2008) 1915–1923

Contents lists available at ScienceDirect

Pattern Recognition Letters

journal homepage: www.elsevier.com/locate/patrec

A region-based GLRT detection of oil spills in SAR images

Lena Chang [a,*], Z.S. Tang [b], S.H. Chang [b], Yang-Lang Chang [c]

[a] Department of Communications and Guidance Engineering, National Taiwan Ocean University, Taiwan, ROC
[b] Department of Electrical Engineering, National Taiwan Ocean University, Taiwan, ROC
[c] Department of Electrical Engineering, National Taipei University of Technology, Taiwan, ROC

ARTICLE INFO

Article history:
Received 29 April 2007
Received in revised form 20 March 2008
Available online 7 June 2008

Communicated by F.Y. Shih

Keywords:
Oil spills
SAR image
Image segmentation
Generalizes likelihood ratio test (GLRT)
Constant false alarm ratio (CFAR)

ABSTRACT

In the study, we propose a fast region-based method for the detection of oil spills in SAR images. The proposed method combines the image segmentation technique and conventional detection theory to improve the accuracy of oil spills detection. From the image statistical characteristics, we first segment the image into regions by using moment preserving method. Then, to get a more integrated segmentation result, we adopt *N*-nearest-neighbor rule to merge the image regions according to their spatial correlation. Performing the split and merge procedure, we can partition the image into oil-polluted and sea reflection regions, respectively. Based on the segmentation results, we build data models of oil spills and approximate them by using normal distributions. Employing the built oil spills model and the generalized likelihood ratio test (GLRT) detection theory, we derive a closed form solution for oil spills detection. Our proposed method possesses a smaller variance and can reduce the confusion interval in decision. Moreover, we adopt the sample average of image region to reduce the computation complexity. The false alarm rate and oil spills detection probability of the proposed method are derived theoretically. Under the criterion of constant false alarm ratio (CFAR), we determine the threshold of the decision rule automatically. Simulation results performed on ERS2-SAR images have demonstrated the efficiency of the proposed approach.

1. Introduction

Recently, the oil pollution in the ocean becomes an urgent topic in the environmental protection. Especially, oil spills caused by intentional or accidental emission has seriously affected wildlife and marine ecosystem. Many ocean phenomena, such as wind spreads the spills quickly and creates a clutter, generate look-alike oil spills in the SAR images. In addition, electromagnetic echoes cause the multiplicative speckle noise. These reasons make the oil spills detection more difficult. Thus, due to the versatility and complexity of the oil pollution, the detection of oil spills is a challenging task for the past years.

The effects of oil spills have been widely studied by various viewpoints with several methods (experimental and theoretical studies) for control and prevention purposes. Remote sensing has proved to be a powerful tool to study ocean dynamics and detection of oil spills (Gade et al., 2000; Bentz and Miranda, 2001). Optical, radiometer, and radar systems have been employed for the detection of oil spills in the sea. In particular, synthetic aperture radar (SAR) image has been shown to be very useful in oil spills monitoring due to its high resolution and wide coverage areas even under unfavorable weather conditions, day and night.

Different systems have been proposed for detecting the oil spills by using SAR images. Since radar is sensitive to surface roughness, oil spills are seen smoother than a clean sea surface and result in a darker area in SAR image. Thus, there are many oil detection algorithms based on thresholding techniques (Bjerde et al., 1993; Fiscella et al., 2000; Solberg and Solberg, 1999). Fiscella et al. (2000) proposed a probabilistic approach which utilized a priori classification probability as a threshold to distinguish oil spills from other similar oceanic features in marine SAR images. Bjerde et al. (1993), Solberg and Solberg (1999) presented algorithms for detection of dark spots are based on adaptive thresholding which is based on an estimate of local mean of the typical backscatter level. Since the selection of threshold has direct influence on segmentation precision and accuracy of the following detection, the techniques (Bjerde et al., 1993; Fiscella et al., 2000; Solberg and Solberg, 1999) require tedious trials in adjustment to obtain a reasonable threshold.

Although the computational efficiency, these thresholding approaches may be sensitive to data inhomogeneities. Some automatic detection algorithms are developed to improve the detection. Lombardo et al. (2000), Bandiera et al. (2003) resort to both multi-frequency and multi-polarization data and Mercier et al. (2003), Mercier and Girard-Ardhuin (2005) utilize the multi-scale strategy for oil spill detection. Recently, Tello et al. (2005a), Tello et al. (2005b) have proposed novel algorithms based

* Corresponding author. Fax: +886 2 23652680.
E-mail address: lenachang@mail.ntou.edu.tw (L. Chang).

0167-8655/$ - see front matter © 2008 Elsevier B.V. All rights reserved.
doi:10.1016/j.patrec.2008.05.022

on time frequency methods, and a semi-supervised detection (Mercier and Girard-Ardhuin, 2006) is proposed using a kernel-based abnormal detection into the wavelet decomposition of a SAR image. A generalized likelihood ratio test (GLRT) based edge detector for polarimetric SAR images has been designed in (Bandiera and Ricci, 2005), which can be used to as the first stage of a system for identification and monitoring of oil spills. Besides, other neural network approaches (Del Frate et al., 2000; Del Frate and Salvatori, 2004) are proposed to alleviate the complex process in developing classification rules and many nonlinear factors involved in Bayesian or statistically based decision methods. Recently, some automatic detection systems (Solberg et al., 2007; Brekke and Solberg, 2005) for oil spills employ the prior information to increase oil detection accuracy.

In the studies, we propose a fast region-based detection algorithm of oil spills in SAR images by using the image segmentation technique. To remove the speckle noise in SAR image, we preprocess the image by using some image enhancement techniques, such as the median filter. Then, an efficient segmentation technique based on the moment preserving principle (Tsai, 1985; Lau et al., 2004) is proposed, which partitions the original image into regions according to the moment statistics of pixel data. These regions are associated with different local terrain characteristics of image, like oil spills, look-alikes and sea reflections. Comparing with Bjerde et al. (1993), Fiscella et al. (2000), Solberg and Solberg (1999), this moment-preserving thresholding can determine the self-adaptive threshold automatically. From the experiments in Section 4, we understand that the moment preserving thresholding technique can distinguish the oil spills from the unpolluted sea areas. Based on the segmentation results, then, we present an oil spills detection algorithm, which involves: data modeling of the oil-polluted image data, and the development of an automatic decision rule. The data modeling involves the procedure, which is supervised by an operator to discriminate between oil spills and look-alikes and extracts the oil feature from the segmented results of training images. From the experimented results and central limit theorem, we approximate the distribution of oil-polluted data by using normal distributions. Experiment results show that many practical factors such as SAR satellite image capturing time, ocean temperature, wind direction and wind speed (Solberg and Solberg, 1996; Singh et al., 1986), will affect the oil spills distributions. In the automatic oil spills detection procedure, we derive a closed form solution based on the built oil spills models and the GLRT detection theory (Kay, 1998). In addition, the criterion of constant false alarm ratio (CFAR) is used to determine the threshold of the decision rule automatically. Simulations validate the detection efficiency of the proposed scheme, even for untrained images.

The remainder of the paper is organized as follows: the model of oil spills in SAR images are developed in Section 2. In Section 3, we propose the oil spills detection algorithm by using GLRT detection theory. Then, experimental results and discussions are shown in Section 4. Finally, Section 5 draws the conclusions.

2. Oil spills modeling

In this section, the models of the oil spills in SAR images are developed. We partition the SAR images into the regions according to their corresponding local terrain and statistical characteristics. From the segmentation results, we extract the features of oil spills and then develop the corresponding data models.

We first split the image by utilizing a thresholding technique with the threshold determined by moment preserving method (Tsai, 1985). The ith-order moment of image $f(x,y)$, denoted by m_i, is defined as

$$m_i = \frac{1}{MN}\sum_{x=1}^{M}\sum_{y=1}^{N} f^i(x,y) \quad i = 0,1,2,3,\ldots. \tag{1}$$

In performing binary segmentation, the moment preserving method determines the best threshold and divides the image into two regions with represented gray levels, z_0 and z_1, respectively, which make the moments invariant during segmentation. That is,

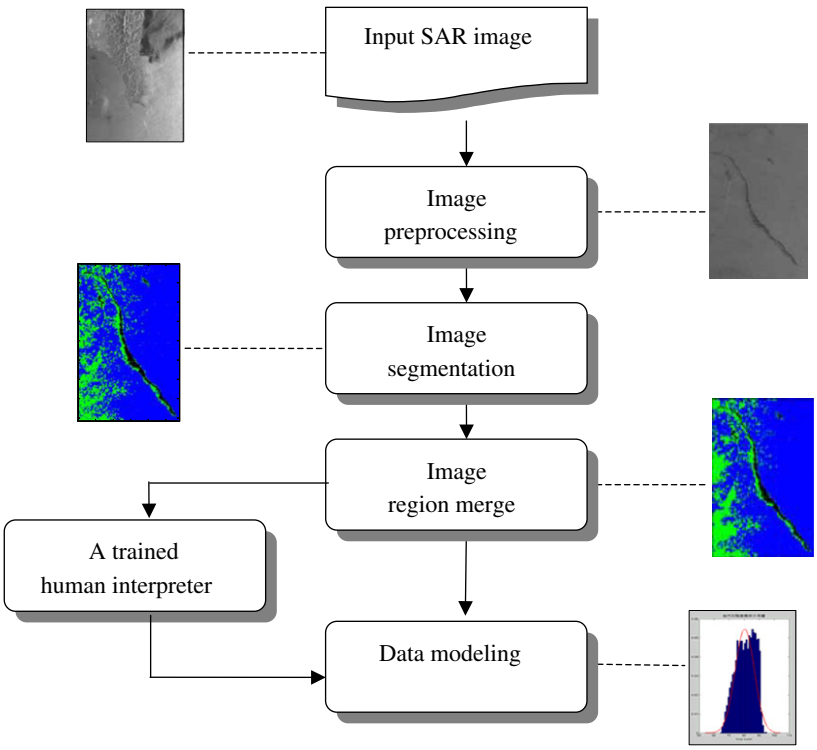

Fig. 1. Flow chart of data modeling.

$$m_i = \sum_{j=0}^{1} p_j z_j^i \quad i = 0, 1, 2, 3, \ldots, \tag{2}$$

where p_j is the proportion of pixel of gray level z_j. By solving (2), p_0 is first found and the desired threshold t is determined by the histogram of the original image to satisfy

$$p_0 = \sum_{i \geqslant t} h_i, \tag{3}$$

where h_i is the proportion of pixel of gray level i in the original image.

The above splitting approach which partitions the image based on pixel statistics may results in small isolated regions. To get a more integrated segmentation result and utilize high correlation of images in spatial domain, we consider the local stationary characteristics of images and further merge the isolated regions by N-nearest-neighbor rule (Kay, 1998). N-nearest-neighbor rule assigns the class of each pixel as the most frequent class among its N-neighbors. Suppose each pixel, x, as a random variable from class ω_i, $i = 1, \ldots, L$. L is the number of classes. According to N-nearest-neighbor rule, x is assigned to class ω_j, if the majority of the N-nearest-neighbors belong to ω_j. In the simulations, 8-nearest-neighbors are considered and N is chosen to be 8.

According to the above segmentation results, a trained human interpreter discriminates the oil-polluted areas in the training images. Some parameters associated with the oil spills, such as mean and variance, are estimated to build the corresponding statistical models. Lombardo et al. (2000) showed that the distribution of SAR image is similar to Gamma distribution. However, based on the "Central Limit Theorem", if the samples are large enough, the distributed will approach the normal distribution. In addition, we analyzed the collected oil spills and sea reflections from ERS-2 SAR images, with histograms of a typical image shown in Fig. 2. We observed that the histograms of oil spills and sea reflections are extremely close to normal distributions. Therefore, to simplify the analysis, we approximate oil spills and sea data model by the normal distributions with probability density function (pdf) as follows:

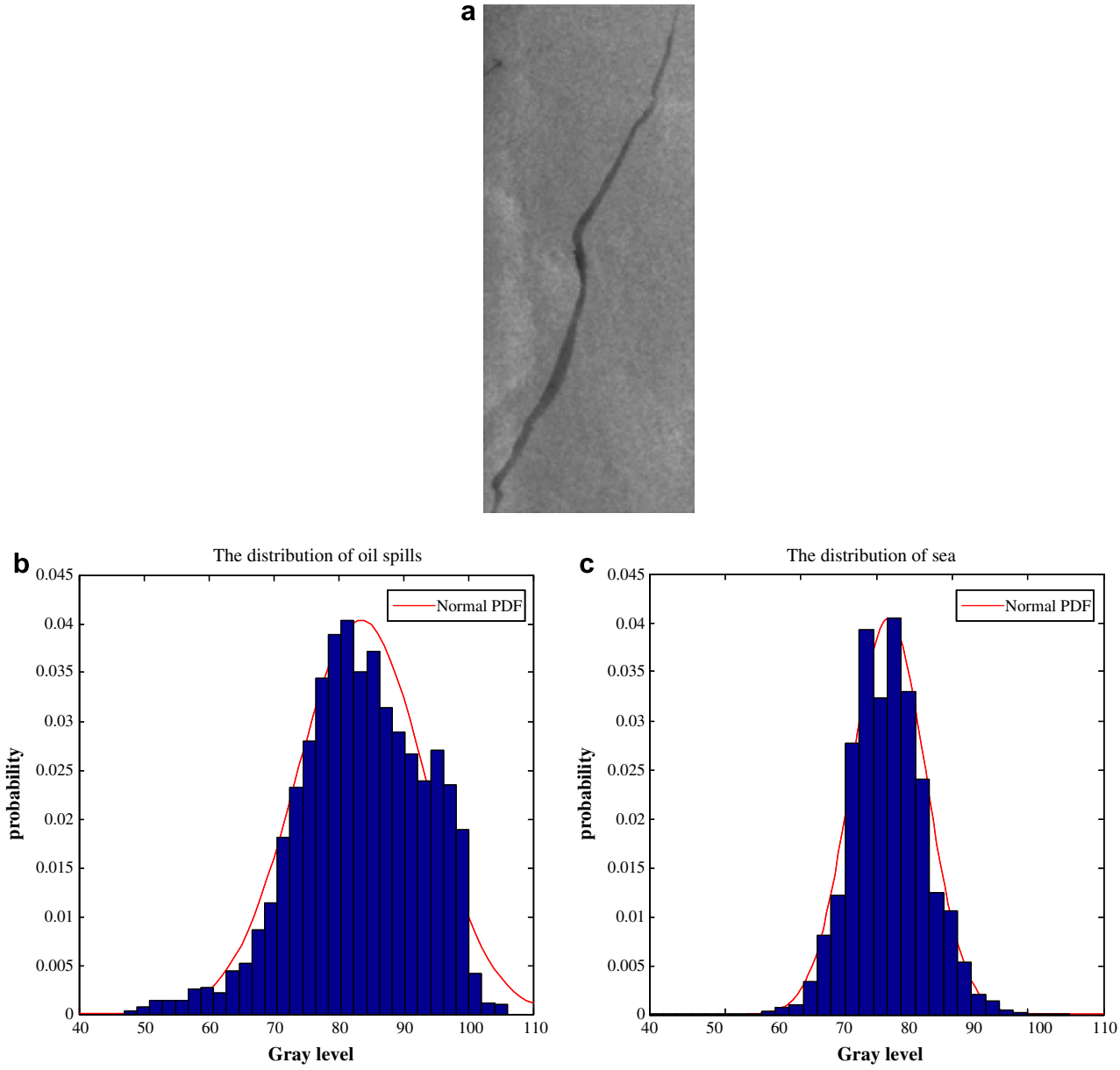

Fig. 2. Histograms of oil spills and sea reflections: (a) SAR image; (b) histogram of oil spills; and (c) histogram of sea reflections.

$$f_X(x) = \frac{1}{\sqrt{2\pi}\sigma} \exp\left[-\frac{1}{2}\left(\frac{x-\mu}{\sigma}\right)^2\right], \quad (4)$$

where μ is mean and σ^2 is variance.

The procedure of data modeling of oil spills shown in Fig. 1, is summarized as follows:

Step 1: Preprocess image by applying some image enhancement techniques. In the study, we utilize median filter to suppress multiplicative speckle noise in the SAR image. The median element of scanning window replaces the center value of image block.

Step 2: Split image into regions. Utilize moment-preserving method to determine a threshold and partition the image into regions according to their moment statistics.

Step 3: Merge the image regions in step 2 according to the local stationary characteristics by using N-nearest-neighbor search rule.

Step 4: Build the data model of oil spills. Approximate oil spills and sea data model by the normal distributions with mean and variance estimated from the segmented results of training images.

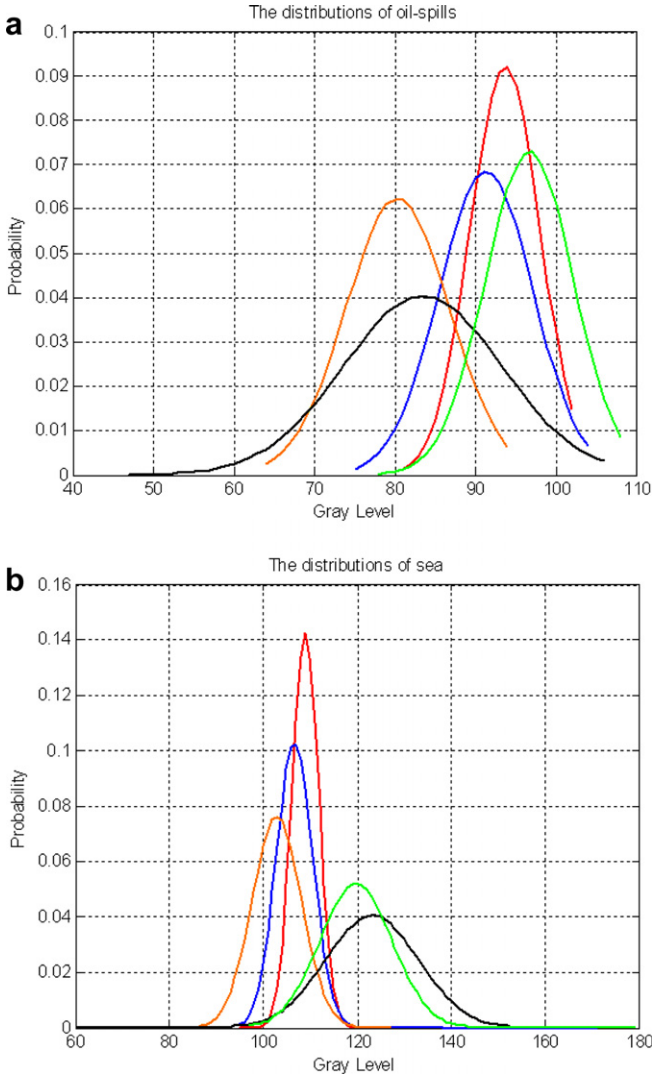

Fig. 3. Distributions of oil spills and sea reflections of 5 test SAR images: (a) oil spills and (b) sea reflections.

Concerning the computation complexity of proposed method, it requires $3MN$ multiplications in determining the moment-preserving threshold and $MN \times O(3\log 3)$ addition operations in steps 1 and 3, if the image size is $M \times N$, the block size in step 1 is chosen to be 3×3 and the 8-nearest-neighbors are considered in step 3. And it takes $M \times N$ multiplications to estimate the mean and variance in building the data model. Generally speaking, the computations required in the proposed method are proportional to the image data size.

In the experiments, ERS-2 SAR images are employed to build the data modeling. Images are first segmented into regions according to steps 2 and 3. Then the oil-polluted areas are determined by human judgment. From the statistics distributions of oil-polluted and sea reflections of five test images shown in Fig. 3, we observed that the oil spills and sea reflections are distributed separately. This result encourages us to derive an automatic oil spills decision rule from distributions. We also found that the pdfs of oil spills from different images are distributed differently. Since the SAR signatures of oil spills depend on external conditions, such as wind speed, wave height, oil released from a stationary object or a moving vessel, and the amount of oil involved, these versatile situations of oil spills result in the different statistical distributions.

3. Oil spills detection

As we learn from the experimental results in Section 2, the corresponding distributions of oil spills and sea reflections are separate. From the distributions in Fig. 3, we see the difference in mean values of probability distributions of the oil spills and sea is relatively large, and their associated variances are also large. Thus, there is a significant region of confusion for oil spills detection.

To improve the oil spills detection efficiency, in our study, we propose a region-based detection scheme. After the image segmentation, image belonged to the same region should have the similar statistical characteristics. As we average the image data with one region, x_i, and get a sample average

$$\bar{x} = \frac{1}{N}\sum x_i. \quad (5)$$

If the distribution of x_i is normal $N(\mu, \sigma^2)$, with mean μ and variance σ^2, the distribution of $\bar{x}$ is also normal with the same mean μ but the variance is reduced to σ^2/N, where N is the pixel number in the region. Since the sample average of each region has smaller variance, the separation of distributions of $\overline{x_o}$ and $\overline{x_s}$ will increase, where $\overline{x_o}$ and $\overline{x_s}$ are the sample averages corresponding to the oil spills and sea reflections regions, respectively. In addition, the larger separation of distributions is the smaller the confusion region will be. Therefore, instead of image pixels or blocks, our detection scheme is region-based.

After the image has been partitioned into regions by moment preserving principle, we further search the discontinuous and isolated regions using region growing method (Gonzalez and Woods, 2002). These isolated regions will be used in our proposed detection scheme to get oil spills.

From the discussions in the previous section, the parameters of the pdfs in (4) corresponding oil spills or sea are different for each image. Under the situation of the unknown parameters, we apply the generalized likelihood ratio test (GLRT) (Kay, 1998) to determine each isolated region being oil spill or not. The GLRT is

$$\Lambda_G(X) = \frac{\prod_{i=1}^{N} P(x_i|\hat{\mu}_1, \hat{\sigma}_1^2, H_1)}{\prod_{i=1}^{N} P(x_i|\hat{\mu}_2, \hat{\sigma}_2^2, H_2)} \underset{H_2}{\overset{H_1}{\gtrless}} \eta, \quad (6)$$

where x_i, $i = 1,\ldots,N$ are the image pixels in the isolated region, H_1 and H_2 are the hypotheses of oil spills and sea, respectively, and η

is a threshold value. In (6), the estimated parameters $\hat{\mu}_1$ and $\hat{\sigma}_1^2$ maximize the conditional pdf $\prod_{i=1}^{N} P(x_i|\hat{\mu}_1, \hat{\sigma}_1^2, H_1)$. That means if the hypothesis H_1 is true, $\hat{\mu}_1$ and $\hat{\sigma}_1^2$ are interpreted as the parameter values most likely to be responsible for the observed data $x_1, \ldots, x_N$. Similarly, if the hypothesis H_2 is true, parameters $\hat{\mu}_2$ and $\hat{\sigma}_2^2$ maximize the conditional pdf $\prod_{i=1}^{N} P(x_i|\hat{\mu}_2, \hat{\sigma}_2^2, H_2)$. If the image is determined to be sea reflections, the observed data $x_1, \ldots, x_N$ most likely come from distribution $N(\hat{\mu}_2, \hat{\sigma}_2^2)$. Thus, we search the most possible parameters $(\hat{\mu}_1, \hat{\sigma}_1^2)$ and $(\hat{\mu}_2, \hat{\sigma}_2^2)$ from the data models built in the previous section.

To reduce the computation complexity, the proposed region-based detection method is further simplified by utilizing the sample average $\bar{x}$ in each region to make a decision. The GLRT in (6) is modified to be

$$\Lambda_G(\bar{x}) = \frac{P(\bar{x}|\hat{\mu}_1, \hat{\sigma}_1^2, H_1)}{P(\bar{x}|\hat{\mu}_2, \hat{\sigma}_2^2, H_2)} \underset{H_2}{\overset{H_1}{\gtrless}} \eta, \tag{7}$$

where $P(\bar{x}|\hat{\mu}_i, \hat{\sigma}_i^2, H_i)$ is normal distribution, $N(\hat{\mu}_i, \hat{\sigma}_i'^2)$ with mean $\hat{\mu}_i$ and variance $\hat{\sigma}_i'^2 = \hat{\sigma}_i^2/N$, for $i = 1,2$. Thus, (7) becomes

$$\Lambda_G(\bar{x}) = \frac{\hat{\sigma}_2'}{\hat{\sigma}_1'} \exp\left(-\frac{1}{2}\left(\frac{\bar{x}-\hat{\mu}_1}{\hat{\sigma}_1'}\right)^2 + \frac{1}{2}\left(\frac{\bar{x}-\hat{\mu}_2}{\hat{\sigma}_2'}\right)^2\right) \underset{H_2}{\overset{H_1}{\gtrless}} \eta, \tag{8}$$

(8) can be simplified as

$$|\bar{x} - \mu| \underset{H_2}{\overset{H_1}{\gtrless}} \gamma, \quad \text{if } \delta > 0, \tag{9}$$

where $\frac{1}{\delta} = \frac{1}{\sigma_2'^2} - \frac{1}{\sigma_1'^2}$, $\mu = \left(\frac{\hat{\mu}_2}{\sigma_2'^2} - \frac{\hat{\mu}_1}{\sigma_1'^2}\right)\delta$ and γ represents a threshold. For $\delta < 0$, the decision result of (9) will be reversed. According (9), we determine whether the image region is oil spills or not.

However, the performance of above decision scheme depends on the selection of the threshold γ. For a common cost function,

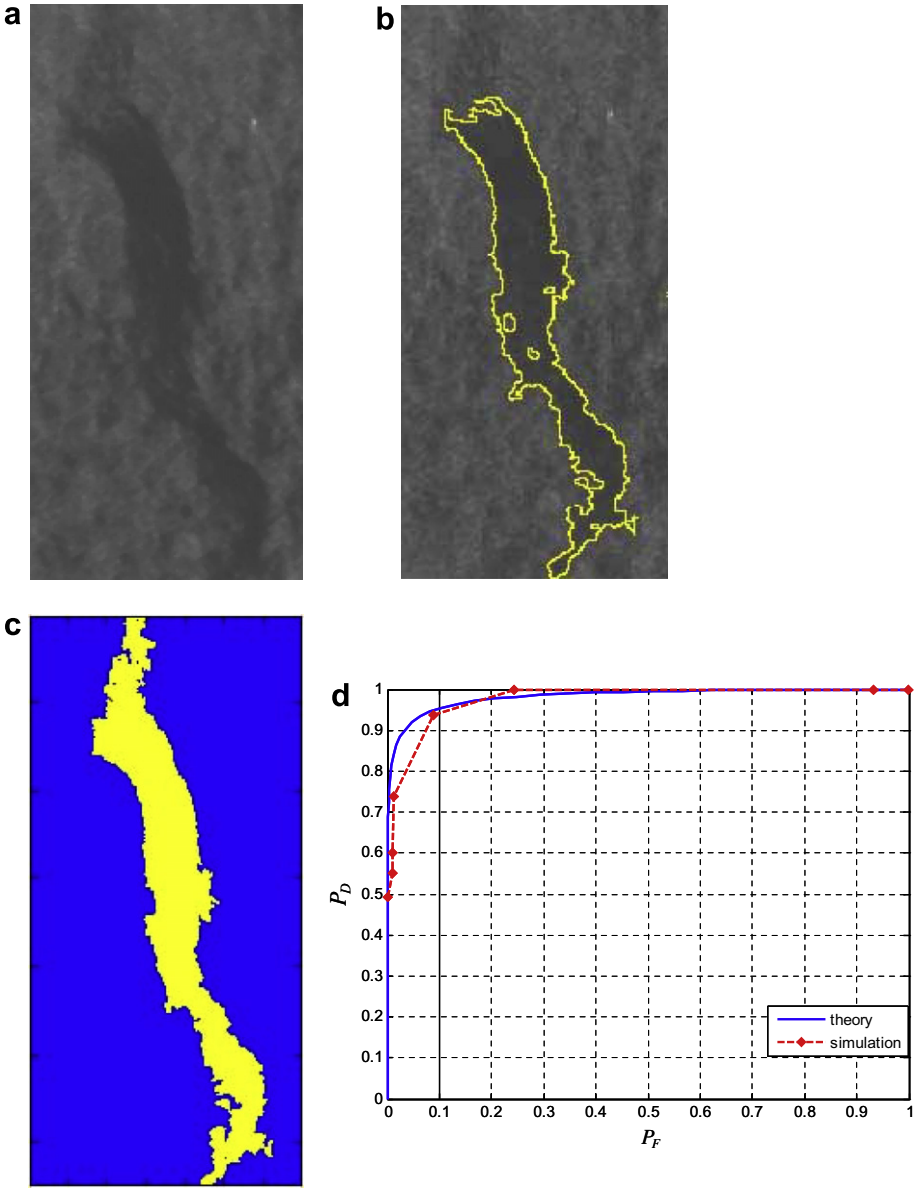

Fig. 4. Detection results of one study area extracted from ERS-2 SAR image acquired on December 2nd, 1999: (a) original image; (b) detection results by the proposed method; (c) detection results by human judgment; and (d) ROC curves.

the determination of the threshold is difficult in many situations. In our study, we select the threshold automatically by using the constant false alarm ratio (CFAR) criterion. While making decision in accordance with (9), the false alarm rate which gives the probability of sea reflection mistaken to be oil spills, is

$$P_F = \int_{-\infty}^{-\gamma} P[y|H_2]\mathrm{d}y + \int_{\gamma}^{\infty} P[y|H_2]\mathrm{d}y. \tag{10}$$

In (10), $y = \bar{x} - \mu$, and $P[y|H_2]$ is distributed to be $N(\mu_y, \sigma_y)$ with $\mu_y = \hat{\mu}_2 - \mu$, and $\sigma_y = \sigma_2' \cdot$ (10) can be simplified as

$$P_F = erfc\left(\frac{\gamma + \mu_y}{\sigma_y}\right) + erfc\left(\frac{\gamma - \mu_y}{\sigma_y}\right), \tag{11}$$

where *erfc* is the complementary error function.

Utilizing the CFAR criterion, we can calculate the threshold γ with P_F equal to a constant. Moreover, under the CFAR criterion, we can calculate the oil spills detection probability, P_D as

$$P_D = \int_{-\infty}^{-\gamma} P[z|H_1]\ \mathrm{d}z + \int_{\gamma}^{\infty} P[z|H_1]\ \mathrm{d}z, \tag{12}$$

where $z = \bar{x} - \mu$. If the image region comes from the oil spills, $P[z|H_1]$ has a distribution $N(\mu_z, \sigma_z)$, with $\mu_z = \hat{\mu}_1 - \mu$ and $\sigma_z = \hat{\sigma}_1'$. P_D in (12) is simplified as

$$P_D = erfc\left(\frac{\gamma + \mu_z}{\sigma_z}\right) + erfc\left(\frac{\gamma - \mu_z}{\sigma_z}\right). \tag{13}$$

Thus, we may evaluate the performance of the detection scheme in (9) by the detection probability in (13).

4. Experiment results and discussions

In this section, simulations are presented to show the efficiency of the proposed detection method. We have conducted the experiments on the ERS-2 SAR images. In simulations, the detection results of training images which have been applied to build the data

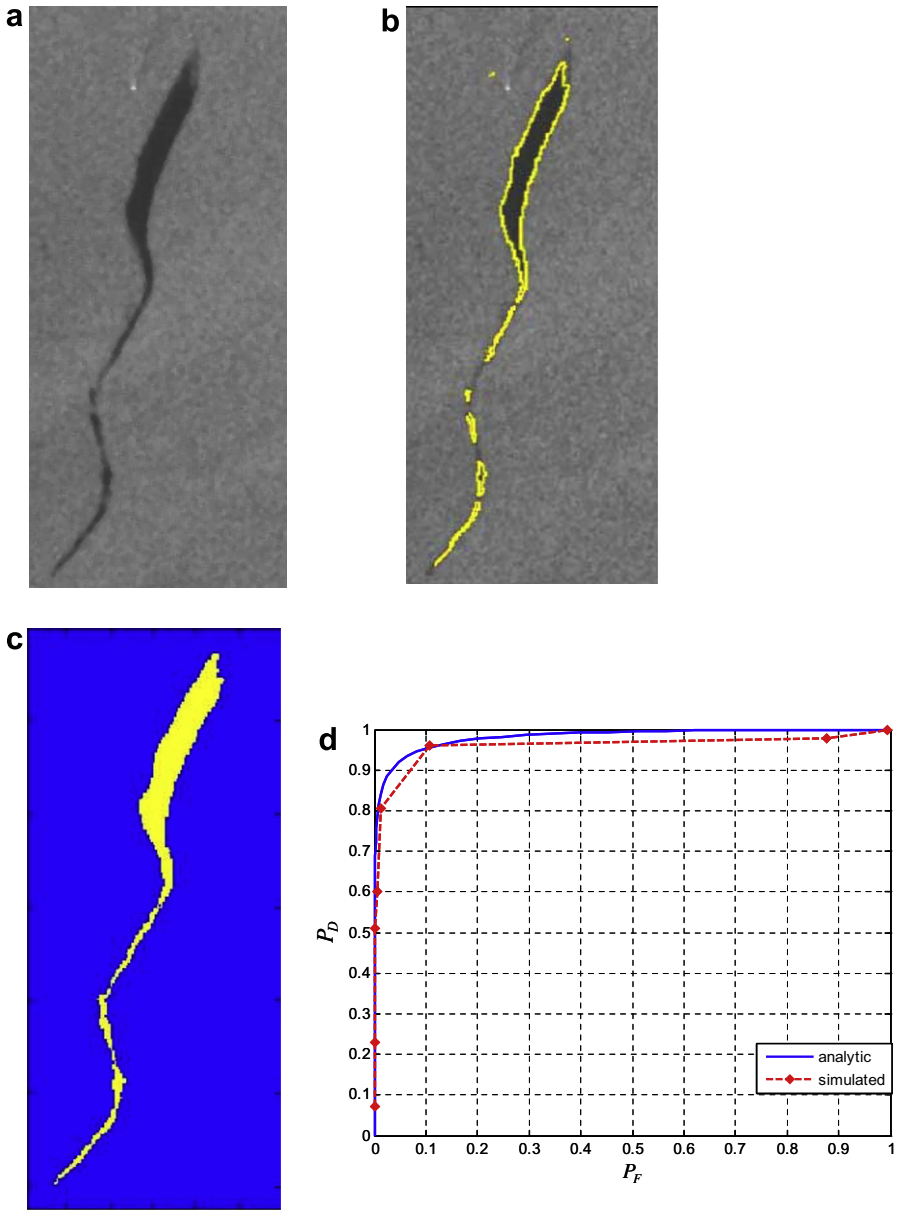

Fig. 5. Detection results of one study area extracted from ERS-2 SAR image acquired on July 15th in 1999: (a) original image; (b) detection results by the proposed method; (c) detection results by human judgment; and (d) ROC curves.

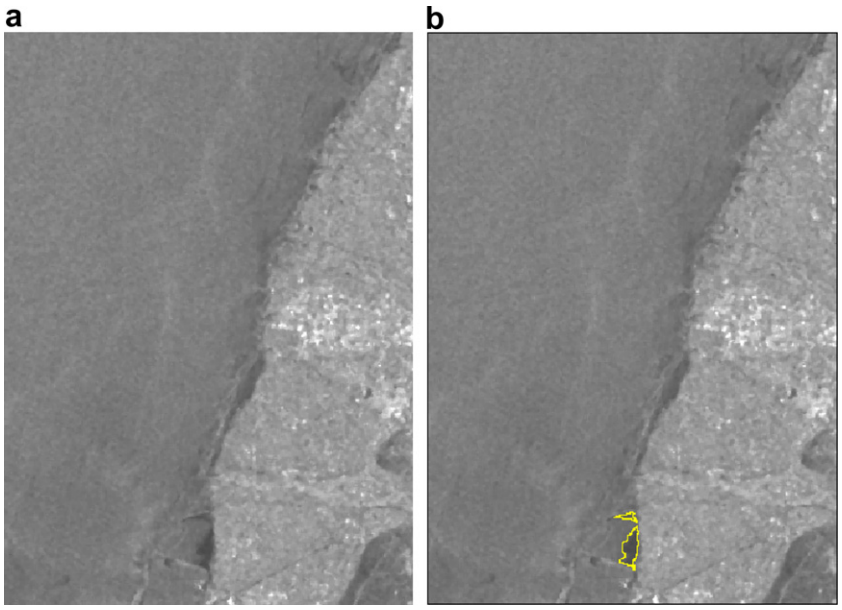

Fig. 6. Detection results of one study area from ERS-2 SAR image dated on November 27th in 1997: (a) original image and (b) detection results.

models, and untrained images are presented to evaluate the performance of the proposed scheme.

4.1. Experiment 1

We first investigate the performance of the proposed detection method on training images. In the experiment, data models of oil spills and sea reflections are built from training sets collected from oil-polluted and unpolluted sea area of 10 training images. To alleviate insufficiency of training images, we pre-segment each training image into regions, and the data in each region is applied for the data modeling. By this way, we create approximately 4000 regions as training sets.

This example that was chosen occurred in December 1999 near the Kaohsiung Harbor in Taiwan. An ERS-2 SAR image was acquired on December 2nd, which was one day after the oil spills accident which a Panama oil tanker occurred near N22°40″ E120°05″ on December 1st, 1999.

One oil-polluted study area of the extracted SAR image is shown in Fig. 4a. Under the CFAR value equal to 8%, the detected results of oil spills circled by yellow[1] curves are given in Fig. 4b. To examine the detection efficiency, we compare the results in Fig. 4b with Fig. 4c in which the oil spills associated with yellow-colored regions are determined by one experienced human. The figures indicate that the detection results of the proposed method are close to human judgment. Most of oil spills are detected accurately except that some small light dark areas are detected improperly. We calculated the probability of error difference between Fig. 4b and c as 0.23%. Furthermore, we evaluate the detection performance by the ROC (receiver operation characteristic) curve. The ROC curves obtained from the simulated results and analytical P_F and P_D in (11) and (13) for varied threshold γ are illustrated in Fig. 4d. The simulated P_F and P_D are measured by comparing the detection results from (9) and those by human judgment. This figure shows that the analytic and the simulated ROC curves match closely. Furthermore, we can find that the detection probability P_D is larger than 90% when P_F is equal to 8%. Thus we choose CFAR value as 8% in our experiments.

[1] For interpretation of color in Fig. 4, the reader is referred to the web version of this article.

4.2. Experiment 2

We examine the detection efficiency of the proposed method on untrained images. An ER2-SAR image acquired on July 15th in 1999 was used in the experiment. A study area of the image given in Fig. 5a contains a long and approximately linear oil spills. Fig. 5b and c shows the detection results of the proposed method and human judgment, respectively. The proposed scheme yields similar detection results as judged by human. Comparing the results in Fig. 5b and c, we obtain that the probability of the error difference between them is 0.86%. From Fig. 5b, we observe that there are some false detection areas near a small white point which is located ahead of the dark oil-polluted area and represents a sailing vessel. In addition, some oil-polluted areas with light gray level are missed in detection. On average, most of the oil-polluted areas are detected accurately. The ROC curves given in Fig. 5d show the efficiency of the proposed detection method for untrained images.

Furthermore, to verify the performance of the proposed method on the images containing no oil spills, one untrained and clean (without oil polluted) ER2-SAR image acquired on November 27th in 1997 was applied to do the simulation. A study area of the image, given in Fig. 6a, is located in the middle west of Taiwan. Fig. 6b shows the detection results. Although there are some look-alike areas near the coast mistaken to be oil spills, the detection error, about 0.28%, is acceptable. The results validate the detection ability of proposed method on SAR images that do not contain oil spills.

4.3. Experiment 3

Then, we compare the detection results of the proposed method with the well known Canny and Laplace of Gaussian and Difference of Gaussian (LoG/DoG) edge detectors. Canny edge detector which applies 2D Gaussian wavelet transform to extract small-scale features, has been used in the oil spill detection system (Mercier and Girard-Ardhuin, 2006). The detection system of Chen et al. (1997) applied LoG/DoG to the multilayers of the image pyramid to locate the position of oil slicks. In the simulations, we select one SAR image, shown in Fig. 7a, offered by ESA (European Space Agency) website (European Space Agency website) for educational

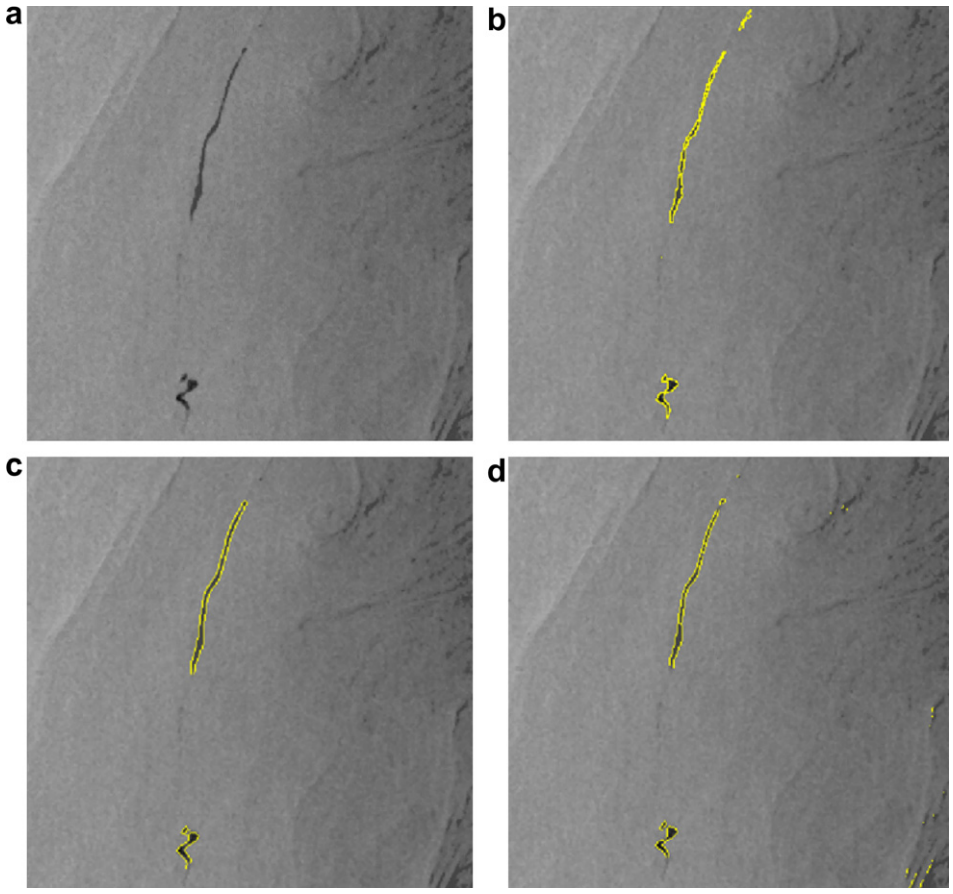

Fig. 7. Detection results of one ESA SAR image acquired on September 17th in 1992 from ESA's website: (a) original image; (b) detection results by the proposed method; (c) detection results by the Canny edge detector; and (d) detection results by the LoG/DoG edge detector.

or informational purposes. The SAR image was acquired on September 17th in 1992 when an oil spill event occurred near the North Sea. There is an obvious oil spill near the North Sea, off the Norwegian coast, which has been confirmed by monitoring aircraft and commercial helicopters. The aerial coverage, thickness and leakage of oil were about 2 km^2, 0.003 mm, and 200 L, respectively.

We can observe that there are an elongate oil spill and some look-alikes in the image of Fig. 7a. The detection results are shown in Fig. 7b–d. From Fig. 7b, we clearly find that the proposed method can detect the main elongate oil spill and the thin oil spill located at the upper side of the elongate oil spill. As shown in Fig. 7c, the Canny approach could detect main oil spill, but the thin oil spill is missed in detection. Observing the results in Fig. 7d, we can see the detection results of the LoG/DoG edge detector approximate to those in Fig. 7c, but some look-alikes are mistaken to be oil spills. Simulation results demonstrate that the proposed method can identifies the oil spills more accurate than the Canny and LoG/DoG approaches.

4.4. Experiment 4

In order to evaluate the performance of proposed detection scheme, we prepare five trained and untrained images, respectively. Each image is partitioned into regions by the proposed segmentation method. Then, we randomly select 50 oil spills and 50 sea reflection sub-regions from each image. Table 1 shows confusion matrices for the classifications based on 10 Monte Carlo Trials. The columns in Table 1 are the actual test classes and the table rows are those determined by the proposed detection method. As illustrated in Table 1, the detection probabilities, $P_D = 1 - P_M$, where P_M is mission probability, are 92.4% and 90% for trained and untrained images, respectively. Since P_D increases consistently with P_F, the oil spills detection probability could be increased by changing the threshold γ in (9) with larger CFAR value. For example, under the CFAR value chosen as 8%, our decision results achieve detection probability P_D larger than 90% for untrained images. This results indicated that the proposed region-based detection method can detect the oil spills effectively and automatically even for untrained images.

Table 1
Confusion matrices for the classifications

Classes	Oil spills		Sea reflection	
	Trained images	Untrained images	Trained images	Untrained images
Oil spills	231	225	8	22
Sea reflection	19	25	242	228
Error probability (P_M/P_F)	7.6%	10%	3.2%	8.8%

P_M denotes the mission probability that oil spills are mistaken to be sea reflection, P_F is the probability of sea reflection mistaken to be oil spills and the total region number is 250 for oil spills and sea reflection in trained and untrained images, respectively.

5. Conclusion

A region-based detection method of oil spills in SAR images has been presented. The method is based on a combination of image segmentation technique and GLRT detection theory. From the seg-

mentation results, we build data models of oil spills and approximate them by using normal distributions. The image pixels within the same region have similar statistical characteristics, and the sample average of image region has a smaller variance. Thus, to improve the detection accuracy, instead of image pixel or block, the sample average of image region is applied as a decision unit. Based on the distributions of oil spills and GLRT detection theory, we develop a region-based decision rule for oil spills detection. The false alarm rate and oil spills detection probability of the proposed method are derived theoretically. Under the criterion of the CFAR, a proper threshold value in the decision rule is determined automatically.

Simulations demonstrate the efficiency of the proposed detection scheme. We conducted experiments to examine the performance of the proposed method by the training and untrained images. Detection results indicated that the proposed region-based detection method can detect the oil spills effectively and automatically even for untrained images. Moreover, the theoretical ROC curves match the simulated results very well. From the ROC curves, we observe that the detection probability P_D is larger than 90% when P_F is chosen around 8%. However, some oil-polluted areas with light gray level are missed or look-alikes are mistaken in the proposed detection scheme. To improve the detection accuracy of the proposed scheme, multi-hypotheses, which contain oil-polluted, unpolluted sea area and look-alikes, and the more useful features of training images for data modeling, will be the main concerns in our future study.

References

Bandiera, F., Ricci, G., 2005. Slicks detection on the sea surface based upon polarimetric SAR data. IEEE Geosci. Remote Sens. Lett. 2 (3), 342–346.

Bandiera, F., Ricci, G., Tesauro, M., 2003. Trained and nontrained CFAR detection of oil slicks on the ocean surface by resorting to SAR data. In: Proc. ISSPA 2003, vol. 1, pp. 353–356.

Bentz, C., Miranda, F.P., 2001. Application of remote sensing data for oil spill monitoring in the Guanabara Bay, Rio de Janeiro, Brazil. In: Proc. IGARSS'2001, vol. 1, pp. 333–335.

Bjerde, K.W., Solberg, A.H.S., Solberg, R., 1993. Oil spill detection in SAR imagery. In: Proc. IGARSS'93, vol. 3, pp. 943–945.

Brekke, C., Solberg, A.H.S., 2005. Oil spill detection by satellite remote sensing. Remote Sens. Environ. 95 (1), 1–13.

Chen, C.F., Chen, K.S., Chang, L.Y., Chen, A.J., 1997. The use of satellite imagery for monitoring coastal environment in Taiwan. In: Proc. IGARSS'1997, vol. 3, pp. 1424–1426.

Del Frate, F., Salvatori, L., 2004. Oil spill detection by means of neural network algorithms: a sensitivity analysis. In: Proc. IGARSS'04, vol. 2, pp. 1370–1373.

Del Frate, F., Petrocchi, A., Lichtenegger, J., Calabresi, G., 2000. Neural networks for oil spill detection using ERS-SAR data. IEEE Trans. Geosci. Remote Sens. 38, 2282–2287.

European Space Agency Website. <http://earth.esa.int/cgi-bin/satimgsql.pl?show_url=522&startframe=0>.

Fiscella, B., Giancaspro, A., Nirchio, F., Pavese, P., Trivero, P., 2000. Oil spill detection using marine SAR images. Internat. J. Remote Sens. 18, 3561–3566.

Gade, M., Scholz, J., Viebahn, C.V., 2000. On the detectability of marine oil pollution in European marginal waters by means of ERS SAR imagery. In: Proc. IGARSS'2000, vol. 6, pp. 2510–2512.

Gonzalez, R.C., Woods, R.E., 2002. Digital Image Processing, second ed. Prentice-Hall.

Kay, S.M., 1998. Fundamentals of Statistical Signal Processing: Detection Theory. Prentice-Hall, Englewood Cliffs, NJ.

Lau, S., Zhang, Q., Luo, F., Wang, Y., Chen, Z., 2004. An improved moment preserving auto threshold image segmentation algorithm. In: Proc. ICIA'04, pp. 316–318.

Lombardo, P., Conte, D.I., Morelli, A., 2000. Comparison of optimized processors for the detection and segmentation of oil slicks with polarimetric SAR images. In: Proc. IGARSS'2000, vol. 7, pp. 2963–2965.

Mercier, G., Girard-Ardhuin, F., 2005. Oil slick detection by sar imagery using support vector machines. In: Proc. IEEE Oceans'05, vol. 1, pp. 90–95.

Mercier, G., Girard-Ardhuin, F., 2006. Partially supervised oil-slick detection by SAR imagery using kernel expansion. IEEE Trans. Geosci. Remote Sens. 44 (10), 2839–2846.

Mercier, G., Derrode, S., Pieczynski, W., Le Caillec, J.-M., Garello, R., 2003. Multiscale oil slick segmentation with Markov chain model. In: Proc. IGARSS'03, vol. 6, pp. 3501–3503.

Singh, K.P., Gray, A.L., Hawkins, R.K., O'Neil, R.A., 1986. The influence of surface oil on C- and Ku-band ocean backscatter. IEEE Trans. Geosci. Remote Sens. GRS-24 (5), 738–744.

Solberg, A.H.S., Solberg, R., 1996. A large-scale evaluation of features for automatic detection of oil spills in ERS SAR images. In: Proc. IGARSS'96, vol. 37, pp. 1484–1486.

Solberg, A.H.S., Solberg, R., 1999. Automatic detection of oil spills in ERS SAR images. In: Proc. IGARSS'99, vol. 37, pp. 1916–1924.

Solberg, A.H.S., Brekke, C., Husoy, P.O., 2007. Oil spill detection in Radarsat and Envisat SAR images. IEEE Trans. Geosci. Remote Sens. 45 (3), 746–754.

Tello, M., López-Martínez, C., Mallorqui, J., 2005a. A novel algorithm for ship detection in SAR imagery based on the wavelet transform. IEEE Geosci. Remote Sens. Lett. 2, 201–205.

Tello, M., López-Martínez, C., Mallorqui, J., 2005b. A novel approach for the detection of punctual isolated targets by means of the wavelet transform. In: Proc. ICIP 2005, vol. 2, pp. 221–224.

Tsai, W.H., 1985. Moment-preserving thresholding: a new approach. Comput. Vision Graph. Image Process. 29, 377–393.